

RSC Advances

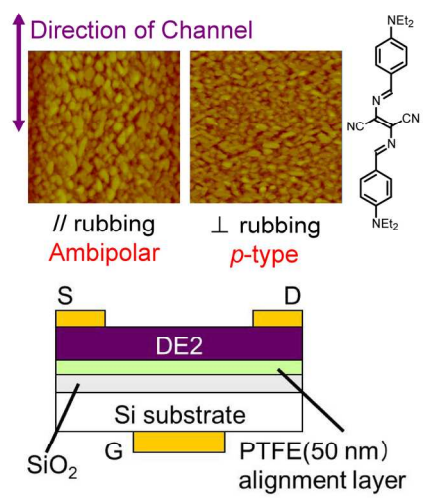


This is an *Accepted Manuscript*, which has been through the Royal Society of Chemistry peer review process and has been accepted for publication.

Accepted Manuscripts are published online shortly after acceptance, before technical editing, formatting and proof reading. Using this free service, authors can make their results available to the community, in citable form, before we publish the edited article. This *Accepted Manuscript* will be replaced by the edited, formatted and paginated article as soon as this is available.

You can find more information about *Accepted Manuscripts* in the [Information for Authors](#).

Please note that technical editing may introduce minor changes to the text and/or graphics, which may alter content. The journal's standard [Terms & Conditions](#) and the [Ethical guidelines](#) still apply. In no event shall the Royal Society of Chemistry be held responsible for any errors or omissions in this *Accepted Manuscript* or any consequences arising from the use of any information it contains.



Graphical abstract
180x135mm (300 x 300 DPI)

ARTICLE

Influence of the grain orientation on the charge transport properties of organic field-effect transistors

Cite this: DOI: 10.1039/x0xx00000x

J.C. Ribierre,^{a,b*} Y. Yokota,^{b,c} M. Sato,^c A. Ishizuka,^{b,c} T. Tanaka,^d S. Watanabe,^{b,e} M. Matsumoto,^e A. Muranaka,^b S. Matsumoto,^{b,c*} M. Uchiyama,^{b,f} and T. Aoyama^{b*}

Received 00th January 2012,
Accepted 00th January 2012

DOI: 10.1039/x0xx00000x

www.rsc.org/

We report on the effects of the crystalline grain orientation on the charge transport properties of a J-aggregate bisazomethine dye (DE2) in thin films. Highly oriented DE2 organic field-effect transistors are fabricated using an insulating alignment layer of poly(tetrafluoroethylene) in the gate dielectric. An enhancement of about one and two orders of magnitude in hole mobility is achieved when the molecules and the crystalline grains are aligned perpendicular and parallel to the transistor channel, respectively. Ambipolar transport is observed only for the parallel alignment. In order to gain additional insights into the role of molecular packing on the charge transport properties of DE2, quantum chemical calculations are carried out to determine and compare the energetic splittings of the highest occupied molecular orbitals (HOMO) and of the lowest unoccupied molecular orbitals (LUMO) in the film. The results provide evidence that DE2 is intrinsically an ambipolar organic semiconductor and demonstrate the important role played by the grain boundary orientation on the charge trapping processes. Overall, the demonstration of field-effect mobilities as high as $0.01 \text{ cm}^2 \text{ V}^{-1} \text{ s}^{-1}$ and the observation of ambipolar transport in our devices represent an obvious milestone for possible use of J-aggregate thin films in organic electronic devices. In addition, this work provides significant insights into the interplay between crystalline grain orientation and ambipolar charge transport properties in organic thin films.

Introduction

Charge transport properties of organic π -conjugated materials have been the subject of intensive studies during the last decades and play an essential role on the performance of a variety of plastic optoelectronic devices.¹ It is well established now that these properties are largely influenced by the electron orbital overlap and thus by the spacing between adjacent conjugated molecules.^{1,2} Different approaches have been developed to control the molecular packing and improve the charge carrier mobilities in organic thin films.³⁻⁶ For example, Giri et al. recently reported a solution-processing technique for organic materials in which lattice strain was used to decrease the π - π stacking distance and enhance charge carrier mobilities.⁷ In the case of polycrystalline organic thin films, grain boundary effects on charge transport and trapping processes can be particularly detrimental to the performance of optoelectronic devices.⁸ Control of the molecular packing and of the orientation of grain boundaries is thus essential for an enhancement of the charge transport properties.⁹⁻¹¹ It has been also demonstrated that changes in molecular packing can lead not only to an improvement of the charge carrier mobilities but also to a majority carrier type conversion.^{2,12-16} In this work, we demonstrate a significant enhancement of the ambipolar charge transport properties in highly oriented organic thin films by controlling the orientation of the molecules and the crystalline grains.

The molecular organization in vapor-deposited J-aggregate organic thin films of N,N'-bis[4-(N,N-diethylamino) benzylidene] diaminomaleonitrile (DE2) as well as their third-order non-linear

optical and photophysical properties have been previously investigated in detail.¹⁷⁻²² The chemical structure of this neutral dye²³ is shown in the inset of Fig. 1a. The good stability of the J-aggregates in DE2 films against heat and moisture was attributed to the non-ionic character of this molecule. Schottky-type organic photovoltaic cells based on J-aggregates DE2 thin films were fabricated and exhibited power conversion efficiencies in the visible region comparable with those typically obtained in metal phthalocyanine thin films.²⁴ The results presented in this work also suggested that DE2 is a p-type organic semiconductor. More recently, top-contact bottom-gate organic field-effect transistors (OFETs) based on vapor deposited J-aggregate DE2 thin films were successfully realized and were found to exhibit hole conduction²⁵ with mobilities as high as $2.4 \times 10^{-4} \text{ cm}^2 \text{ V}^{-1} \text{ s}^{-1}$. Furthermore, DE2 molecules can be highly oriented by depositing the dye on aligned poly(tetrafluoroethylene) (PTFE)^{26,27} layer, thereby forming films with large degrees of in-plane anisotropy and dichroic ratios up to 40.^{21,22} Such a high degree of molecular orientation should have a significant effect on the charge transport properties.

In this manuscript, we report on the fabrication and characterization of DE2 OFETs with a rubbed alignment PTFE layer in the gate dielectric. The results show the crucial role played by the molecular and grain boundary orientation on the charge transport properties of polycrystalline DE2 thin films. In particular, enhancement of the hole field-effect mobility by about two orders of magnitude and ambipolar transport are observed in OFETs with a molecular alignment parallel to the device channel. The ambipolar character of DE2 films is fully supported by quantum chemical

calculation of the energetic splittings of the highest occupied molecular orbitals (HOMO) and of the lowest unoccupied molecular orbitals (LUMO). In particular, 3D calculations were carried out to examine the role of the molecular orientation on the ambipolar charge transport properties of DE2 single crystal. To explain our experimental results in polycrystalline DE2 thin film devices, influence of charge trapping by the grain boundaries on the mobilities must also be taken into account. Overall, our study provides important insights into the interplay among molecular packing, grain boundary orientation and ambipolar charge transport properties. The demonstration of ambipolar transport in J-aggregate DE2 OFETs suggests the possibility to use organic J-aggregates in efficient light-sensing electronic devices.

Experimental

For the absorption spectra measurements, 50 nm thick layers of PTFE with a good uniformity were deposited by thermal evaporation onto precleaned fused silica substrates. The PTFE films were rubbed by a cloth at a pressure of 5 kg/cm² in a given direction at a speed of 5 mm/s.^{21,27} The DE2 thin films were then vapor-deposited on top of the PTFE alignment layers. Absorption spectra were measured using an UV-VIS-NIR scanning absorption spectrophotometer (Shimadzu, UV-3100PC) and a sheet polarizer to control the linear polarization parallel and perpendicular to the sliding direction. The atomic force microscopy (AFM) images were recorded in the tapping mode on a Veeco Dimension 3100 Scanning Probe Microscope with a Nanoscope V controller and equipped with a Si coated cantilever (Veeco, model NCH-W, resonance frequency: 261.9 kHz, spring constant: 29-48 N/m). Silicon wafers with a thermally grown 300 nm thick SiO₂ layer were used as substrates for the top-contact bottom-gate OFETs. The 50 nm thick PTFE dielectric layers and the DE2 films were prepared using exactly the same procedure as above. Gold source/drain electrodes were then evaporated through a shadow mask on top of the DE2 films. Prior to the deposition of the organic dye, the PTFE layers were rubbed in the directions parallel and perpendicular to channel of the devices. In all the devices, the length (L) and the width (W) of the channel are 45 μm and 4 mm, respectively. Electrical properties of the OFETs were characterized using a couple of picoammeter/voltage source units (Keithley, model 6487). The field-effect mobility μ was calculated in the saturation regime using the following equation: $I_d = (W / 2L) \mu C_i (V_g - V_{th})^2$, where I_d is the drain current, C_i is the capacitance density of the gate dielectric taking into account that the dielectric constant of PTFE is about 2.1,²⁸ V_g is the gate voltage and V_{th} is the threshold voltage determined from the plot of $(|I_d|)^{1/2}$ as a function of V_g .

Theoretical Methodology

The charge transport mechanism between molecules can be seen as a charge transfer from a charged donor molecule to a neighboring neutral acceptor molecule.^{2,29-32} As previously described in the literature, the charge hopping rate, noted k_{hop} , in absence of electric field, can be described as:²

$$k_{hop} = \frac{2\pi}{h} t^2 \frac{1}{\sqrt{4\pi\lambda k_B T}} \exp\left[-\frac{\lambda}{4k_B T}\right] \quad (1)$$

where λ is the reorganization energy for the intermolecular charge transfer, T is the temperature and t is the transfer integral, which describes the strength of the electronic interaction between neighboring molecules. The transfer integrals for holes and electrons can be estimated, with the help of the semi-empirical Hartree-Fock-based Zerner's Intermediate Neglect of Differential Overlap (ZINDO/S) method³⁰ using the Gaussian 09 suites of programs³³, by calculating the splittings of the HOMO and LUMO levels upon

interaction in stack of molecules extracted from the crystalline structure of the material. In addition, these quantum chemical calculations can be used to determine the preferential directions for charge transport in films and the relative mobilities of holes and electrons.^{34,35}

In this work, quantum chemical calculations were carried out to understand at a microscopic level the relationships between the molecular packing and the charge transport properties of DE2 thin films. Following the method detailed in previous studies, the semi-empirical Hartree-Fock-based ZINDO/S method was used to calculate the electronic structure of isolated DE2 molecules and of systems composed of dimers or larger 3-dimensional molecular clusters in configurations found in the crystalline structure of DE2 at room temperature. The transfer integrals between adjacent monomers were also evaluated using the PW91 functional and the TZP basis set as implemented in the ADF package³⁶. The calculated values of the HOMO and LUMO splittings in these systems are then compared to discuss about the influence of the molecular orientation on the ambipolar charge transport properties of DE2 films observed experimentally.

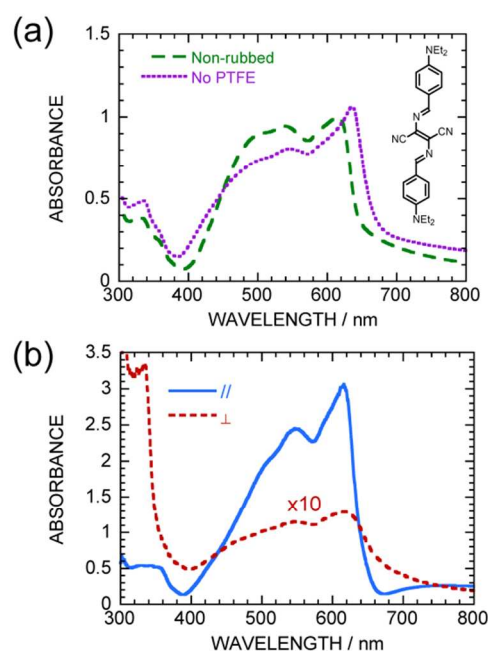


Fig. 1 (a) Absorption spectra of 93 nm thick DE2 films deposited onto either SiO₂ or a 50 nm thick PTFE layer. The chemical structure of DE2 is shown in the inset. (b) Polarized absorption spectra of the highly oriented 93 nm thick DE2 film deposited onto an aligned PTFE layer. Light polarization was either parallel or perpendicular to the aligned PTFE chains.

Results and discussion

Absorption spectra and optical dichroic ratio

Vapor-deposited DE2 films are known to exhibit two phases: a non-aggregate crystalline phase and a J-aggregate phase.²⁵ While the two phases are present in DE2 films thicker than 90 nm, the non-aggregate crystalline phase dominates in thinner films. The absorption features of these two phases has been previously examined in details.^{17,21} Fig. 1a shows the absorption spectrum of a

93 nm thick DE2 thin film vapor-deposited onto a 50 nm thick PTFE layer. This spectrum is compared to that obtained without the PTFE film. Both spectra present similar features. The peak located in the region 530-560 nm is attributed to the absorption from the non-aggregate crystalline phase of the DE2 film. The other peak observed at 600-620 nm is assigned to the absorption of the J-aggregate phase.^{17,21,25} In fact, it should be mentioned that the shape and the position of this J-aggregate peak slightly vary with film thickness, due to a thickness dependence of the J-aggregate formation in DE2 films. A model describing the J-aggregate formation in DE2 has been already proposed, suggesting that the J-aggregates are formed at the top surface of the film when the crystalline grains are sufficiently large to be in contact with each other.³⁷ The differences between the absorption spectra displayed in Figure 1a are presumably due to changes in film morphology and their effects on J-aggregate formation. DE2 thin film was also vapor-deposited onto an alignment PTFE layer. This layer was rubbed in a given direction at constant pressure and speed, in order to orient the PTFE chains parallel to the sliding direction. Fig. 1b shows the absorption spectra of this sample for a polarization of the light parallel and perpendicular to the PTFE chain orientation. The absorbance of the J-band is found to be much higher when the direction of polarization is parallel to the rubbing direction of the PTFE layer. The dichroic ratio between the absorbances measured for parallel and perpendicular polarizations reaches values of 24 and 21 at 616 and 549 nm respectively. Taking into account the fact that the absorption transition dipole moment of the DE2 molecule lies in the direction of its long axis, these results provide evidence that the DE2 molecules are indeed strongly oriented parallel to the PTFE chains in both aggregate and crystalline phases²¹.

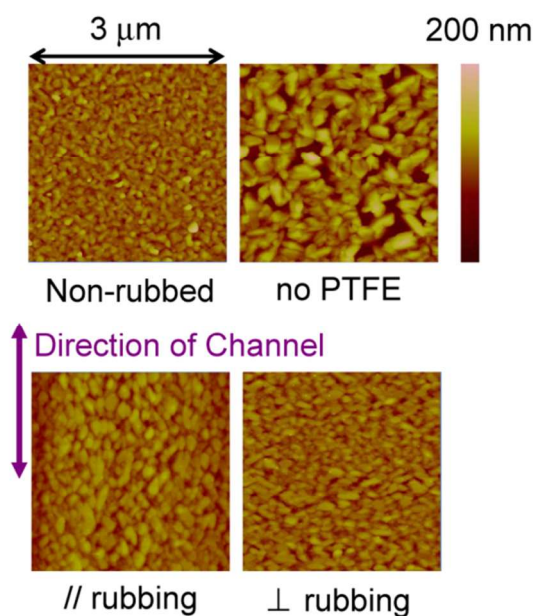


Fig. 2 AFM images of DE2 films used in the devices. The films were prepared onto a PTFE layer with a molecular alignment parallel to the channel, with a molecular alignment perpendicular to the channel and without any alignment. The AFM image of the DE2 film prepared onto SiO₂ is also shown for comparison. The thickness of the four DE2 films was 93 nm.

The film morphology of DE2 films deposited onto glass substrates has been previously investigated in details. It was demonstrated that J-aggregate DE2 films showed heterogeneous film texture with soft and curved crystalline grains as well as unclear grain boundaries. A solvent-vapor treatment was also found to strongly modify the surface morphology of the DE2 film, leading to a fine-grained texture with well-defined grain boundaries. The AFM images displayed in Figure 2 are consistent with these previous observations. Nevertheless, the surface morphology of the J-aggregate DE2 films is clearly affected by the PTFE layer. In particular, the crystalline grains seem to be less isolated in the PTFE cases. These morphological differences can be responsible for the changes observed in the absorption spectra displayed in Fig. 1a. More importantly, the AFM images in Figure 2 show that the crystalline grains are strongly oriented in the rubbing directions. This is in good agreement with the alignment of the DE2 molecules along the direction of the PTFE chains previously evidenced by the absorption spectra measurements. It should be noted that the grain size should be similar in the DE2 films prepared onto the PTFE layer with a molecular alignment parallel and perpendicular to the channel. The little differences observed in Fig. 2 are only due here to the sample dependence of the crystalline grain formation.

The surface roughness of the DE2 films was determined from the AFM images and their values are listed in Table 1. The films deposited on PTFE exhibit a lower roughness than the sample prepared onto SiO₂. In addition, the roughness of the rubbed and non-rubbed DE2 films vapor-deposited on the PTFE layer is nearly identical, indicating that the rubbing does not affect significantly the roughness of the films. To gain further insights into the surface morphology of the DE2 films, the Fourier transforms of the AFM images were calculated in the direction of the device channel and the obtained power spectral densities (PSD) were fitted using a single Gaussian function, which can be expressed as $PSD \approx \exp[-(x-m_0)^2/2v]$, where m_0 and $2v$ correspond to the inverse of the grain size and the dispersion factor of m_0 , respectively. The values of m_0 and $2v$, were evaluated in the 93 nm thick DE2 films and are summarized in Table 1. It can be seen that the grain size is larger and the dispersion factor $2v$ is smaller in the no PTFE case. In the samples prepared onto the PTFE layer, the value of m_0 is significantly lower for the parallel alignment due to the orientation of the crystalline grains in the direction of the channel. Similarly, m_0 is found to be the largest for the perpendicular alignment. These results will be useful to discuss about the influence of the grain boundaries / grain sizes on the charge transport properties of aligned and non-aligned DE2 films.

Table 1 Hole field-effect mobilities in the saturation regime, inverse of the grain size (m_0), dispersion factor of m_0 ($2v$) and RMS roughness (R_q) in 93 nm thick DE2 OFETs with a parallel molecular alignment, a perpendicular alignment, without any alignment, and without PTFE layer.

	Parallel	Perpendicular	Non-rubbed	No PTFE
Mobility ($\text{cm}^2 \text{V}^{-1} \text{s}^{-1}$)	0.006	0.0003	1.1×10^{-5}	2×10^{-5}
Inverse of the grain size (m_0) (μm^{-1})	1.73	3.16	2.78	1.44
Dispersion of m_0 ($2v$) (μm^{-2})	15.7	26.7	30.7	7.21
RMS roughness (R_q) (nm)	13.7	12.0	12.6	27.2

Organic field-effect transistors

The output and transfer characteristics are measured in DE2 OFETs with the PTFE layers rubbed either in the parallel or the perpendicular direction, with no rubbing, and with no PTFE layers. As shown in Fig. 3, the output characteristics of the devices with a molecular orientation perpendicular and parallel to the channel show clear linear and saturation regions for negative drain-source voltages (V_d) and gate voltages (V_g). Similar behavior is observed in OFETs with both non-rubbed PTFE and no PTFE layers. These results indicate that the highly oriented J-aggregate DE2 OFETs operate well in the hole accumulation mode, independently of the molecular orientation. As displayed in Fig. 3, the transfer characteristics measured in DE2 OFETs with parallel and perpendicular molecular orientations for $V_d = -80$ V show a strong drain current (I_d) at negative V_g , which confirms that the devices present good hole transport properties. It is important to emphasize here that while the absorption spectra of DE2 films exhibit a strong influence of the film thickness on the J-aggregate formation, it was previously demonstrated that the hole mobility in DE2 OFETs with a SiO_2 gate dielectric does not vary in films thicker than 90 nm. This behavior was attributed to the fact that the J-aggregates are formed in DE2 films at the surface of the crystalline grains and thus do not affect the semiconductor/gate dielectric interface and the charge transport properties. In that regard, while the formation of J-aggregates in DE2 films plays a major role on their optical properties, its influence on the charge transport properties is negligible in the OFET architecture and does not need to be taken into account to describe the results presented in this work.

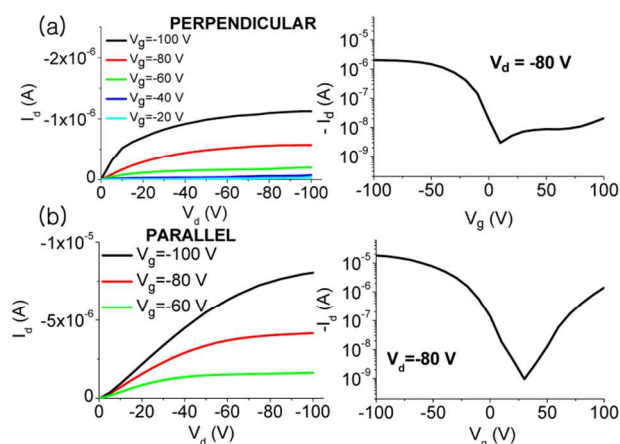


Fig. 3 (a) Output and transfer characteristics of a 150 nm thick DE2 OFET with a molecular alignment perpendicular to the device channel. (b) Output and transfer characteristics of a 190 nm thick DE2 OFET with a parallel orientation. In both cases, the thickness of the PTFE alignment layer is 50 nm. Top contact source/drain electrodes were made of gold. The channel width and length were 4 μm and 45 μm respectively.

Field-effect mobilities are calculated in the saturation region from the transfer characteristics. The averaged values measured in 93 nm thick DE2 OFETs are listed in Table 1. The molecular orientations parallel and perpendicular to the channel lead to hole mobilities of 5.8×10^{-3} and 2.9×10^{-4} $\text{cm}^2 \text{V}^{-1} \text{s}^{-1}$, respectively. It is worth noting here that a chloroform vapor treatment results in an improvement of the device performance, due to an improved molecular packing.²⁵ After such a treatment, hole mobility could be enhanced up to 0.01 $\text{cm}^2 \text{V}^{-1} \text{s}^{-1}$ in DE2 OFETs with a molecular alignment parallel to the channel. Note that a value of about 1×10^{-5} $\text{cm}^2 \text{V}^{-1} \text{s}^{-1}$ is measured

in a device containing a non-rubbed 50 nm PTFE film, which is nearly two times lower than the hole mobility measured in a DE2 OFET with a SiO_2 gate dielectric layer. We also find that the alignment PTFE layer causes significant variations in the threshold voltage (V_{th}) and the drain current on/off ratio ($I_{on/off}$). For example, in the case of a 93 nm thick DE2 film, V_{th} reaches the values of 7 and -11 V and $I_{on/off}$ is measured to be around 10^2 and 10^3 when the molecules are oriented perpendicular and parallel to the channel, respectively. Similar changes in V_{th} and $I_{on/off}$ are observed in devices using DE2 thin films with various thicknesses ranging from 70 to 230 nm. As mentioned above, the integration of a non-rubbed PTFE layer in the DE2 OFETs leads to a decrease of the hole field-effect mobility. This is certainly due to the larger crystalline grain size observed in the no PTFE device, as evidenced by the AFM images in Figure 2. However, a strong enhancement of the hole field-effect mobilities is observed when the DE2 molecules are aligned parallel and perpendicular to the channel. This demonstrates that the rubbed PTFE films are attractive dielectric alignment layers for the realization of OFETs with highly oriented active organic semiconducting thin films.

The observed enhancement of the charge transport properties in highly oriented J-aggregate DE2 OFETs can be due to an increase of the mobilities inside the grains³⁸⁻⁴⁰, the orientation of the grain boundaries^{8,41} or a combination of these two effects. An increase of the mobilities inside the grains is supported by the average values of the grain sizes calculated from the Fourier transforms of the AFM images by fitting the power spectral densities with a single Gaussian function. The results shown in Table 1 indicate that the grain size in the channel direction for the perpendicular alignment is comparable to that of the non-rubbed film. This suggests that enhanced mobilities measured in the perpendicularly aligned DE2 films are due to a molecular packing in the grains more favorable to charge transport. In addition to the anisotropic hole mobility inside the grains, another plausible reason for the enhanced mobilities with the parallel molecular alignment is based on the role played by the orientation of the grain boundaries. It is well known that grain boundaries can induce energy barriers to charge transport, leading to a large decrease of the charge carrier mobilities.⁴²⁻⁴⁵ Similarly to what was observed in a perylene diimide derivative,⁸ it is possible that the grain boundaries in the parallel DE2 devices show a lower degree of molecular misorientations resulting in a smaller barrier to transport. This is highly supported by the variations observed in V_{th} which can arise from the impact of the anisotropy of the DE2 crystalline grains on the charge trapping processes near the dielectric layer interface. As displayed in Fig. 3, an electron current is observed at positive V_g only in the transfer characteristics of the devices with a molecular orientation parallel to the channel. Electron field-effect mobilities up to 7×10^{-4} $\text{cm}^2 \text{V}^{-1} \text{s}^{-1}$ are measured in the saturation regime. These results show an unprecedented way of tuning the ambipolar transport properties via the control of the orientation of the molecules and the crystalline grains within the device channel.

Quantum chemical calculations

To clarify the role of the molecular packing and grain boundaries on the ambipolar charge transport properties of DE2 films, quantum chemical calculations were carried out to determine the electronic structure of DE2 crystal. The crystalline structure of DE2 at room temperature has been already reported in previous works^{18,21}. The DE2 molecules in the crystal present two configurations with different torsion angles and planarity of the benzene rings. As shown in Fig. 4, these two configurations, noted α and β , exhibit slightly different distribution on the HOMO and LUMO. This must be taken

into account in the quantum chemical calculations of the electronic structure of the crystal. From Fig. 5, it can also be seen that each α monolayer is sandwiched between two β layers and that the direction of DE2 molecules is different in two neighboring β monolayers, that we note $\beta 1$ and $\beta 2$. In order to analyze the interactions between all DE2 dimers in such a crystalline structure, the calculation of the HOMO and LUMO splittings must be carried out in several configurations which are shown in Fig. 6 and in Fig. 7.

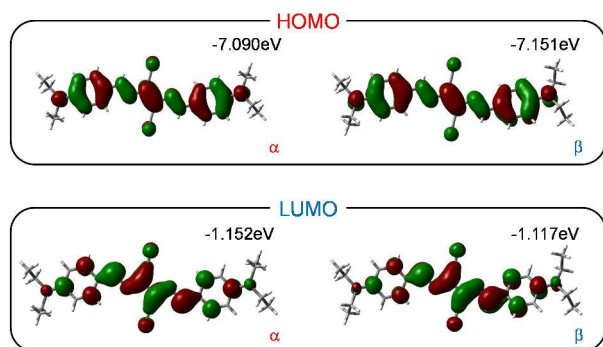


Fig. 4 Calculated HOMO and LUMO of DE2 in the neutral ground-state geometry for the α and β molecular structure.

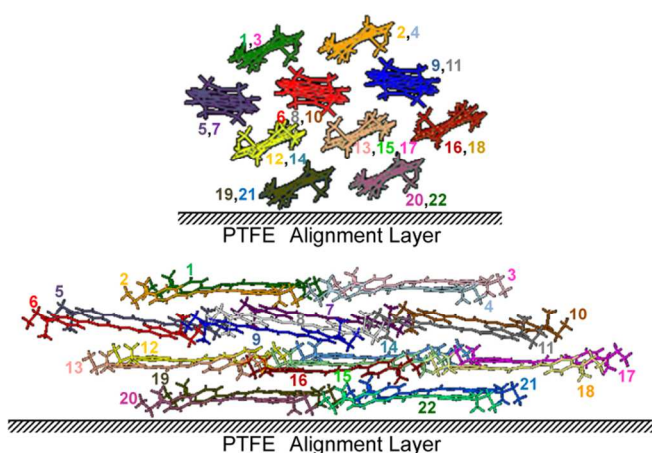
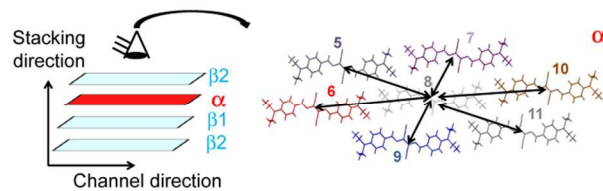


Fig. 5 Schematic representation in three-dimension of the crystalline structure in DE2 thin films deposited onto a PTFE layer. A number is allocated to each molecule shown in these illustrations.

Table 2 shows the HOMO and LUMO splittings calculated for DE2 dimers located either in the α or the β layer. In this case, the interaction was computed between a central molecule (molecule 8 for the α layer and molecule 15 for the β layer) and its neighboring molecules located in the same monolayer. It was found that the HOMO and LUMO splittings resulting from the interactions of dimers either in the α or β layer are small (≤ 16 meV), indicating

(a) Interaction in the single α layer (central molecule : 8)



(b) Interaction in the single β layer (central molecule : 8)

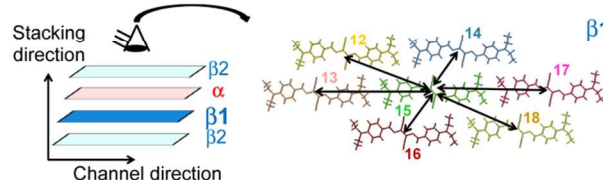
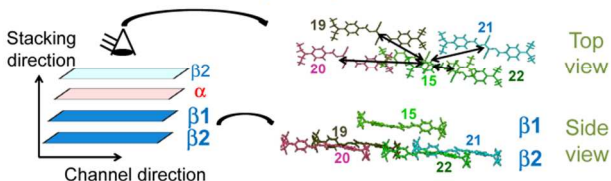


Fig. 6 Schematic representation of the DE2 crystalline structure used for the calculation of the HOMO and LUMO splittings in dimers located in the (a) alpha and (b) beta monolayer. The numbers associated with each molecule correspond to those given in Fig. 5.

(a) Interaction between the $\beta 1$ and $\beta 2$ layer (central molecule : 15)



(b) Interaction between the α and $\beta 1$ layer (central molecule : 15)

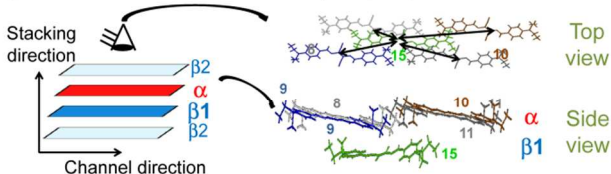


Fig. 7 Schematic representation of the DE2 crystalline structure used for the calculation of the HOMO and LUMO splittings in dimers composed of molecules in two different monolayers. The configurations shown in (a) and (b) were used to characterize the intermolecular interactions between (a) $\beta 1$ and $\beta 2$ monolayers and (b) α and $\beta 1$ monolayers. The numbers associated with each molecule correspond to those given in Fig. 5.

Table 2 Calculated values of the HOMO and LUMO splittings in dimers located either in the same α or β layer. The numbers characterizing the position of each DE2 molecules in the crystalline structure are indicated in Figures 5 and 6.

Dimer	Δ HOMO (meV)	Δ LUMO (meV)
α-α interactions		
8-5,11	4	1
8-6,10	0	0
8-7,9	2	1
β-β interactions		
15-12,18	5	6
15-13,17	3	1
15-14,16	16	3

Table 3 Calculated values of the HOMO and LUMO splittings in dimers composed of molecules located in different monolayers. The numbers characterizing the position of each DE2 molecules in the crystalline structure are indicated in Figures 5 and 7.

Dimer	Δ HOMO (meV)	Δ LUMO (meV)
β1-β2 interactions		
15-19	0	10
15-20	7	1
15-21	3	1
15-22	143	83
α-β1 interactions		
15-8	74	57
15-9	73	16
15-10	51	44
15-11	14	84

that charge transport along the same molecular monolayer is not efficient. In contrast, Table 3 shows significantly higher HOMO and LUMO splitting values for dimers composed of two molecules placed in different monolayers. For instance, in case of an interaction between β 1 and β 2 layers, the dimer composed of the molecules 15 and 22 presents a large overlap of the molecular orbitals, resulting in high HOMO and LUMO splitting values equal to 143 and 83 meV, respectively. The other splittings are much smaller, presumably because the distance between the interacting molecules is significantly larger. For interactions between α and β 1 layers, all the different configurations showed high splitting values. In particular, it can be seen that the dimer 15-8 displays HOMO and LUMO splittings equal to 57 and 74 meV, respectively. However, because the molecular structure of DE2 is different in the α and β layers, some of these dimers do not show symmetrical orbitals, which can lead to overestimated calculated values of the splittings. To overcome this issue related to the energetic mismatch between different monomers, splittings were also calculated using the ADF package. The results obtained with this method are shown in the supplementary information section. These data are consistent with those obtained by the Hartree-Fock-based ZINDO/S approach. The demonstration of the main path for the charge carrier (8-15,22) is confirmed. However, the ADF method shows that in addition the LUMO splitting of the dimer (15-10) is also moderately large, suggesting that this path might be favorable to electron transport. From all these considerations, we can propose that charge transport in DE2 films takes place more effectively between the molecules 8, 15 and 22, indicating that the charge carriers would migrate in the film by zigzagging through this main path. Another important information that can be deduced from these calculations is that DE2 presents the potential of being an ambipolar organic semiconductor. Indeed, LUMO splittings higher than 70 meV calculated in some DE2 dimers are similar to those calculated in n-type fullerene derivatives⁴⁶.

We also calculated the HOMO and LUMO splittings for several molecules selected 3-dimensionally in the DE2 crystal using the Hartree-Fock-based ZINDO/S method. Fig. 8 shows the results obtained by taking DE2 molecules only in the β layers. The HOMO and LUMO splittings obtained for the 4 selected molecules were found to be 153 and 132 meV, respectively. This suggests that ambipolar charge transport could occur in the β layers. When two molecules are then placed sideways, as displayed in Fig. 8, both HOMO and LUMO splittings increase to 220 and 186 meV. On the other hand, by placing one molecule in front and another one behind the four initial DE2 molecules, we found that the HOMO and LUMO splittings yield values of 211 and 148 meV. The higher

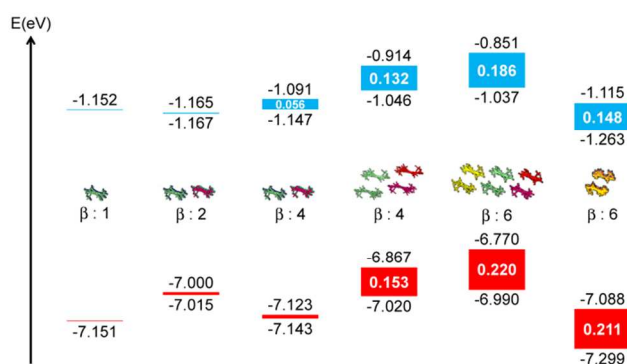


Fig. 8 HOMO and LUMO splittings calculated in 3-dimensional molecular clusters in a β layer in order to simulate the influence of the molecular orientation on the ambipolar charge transport properties.

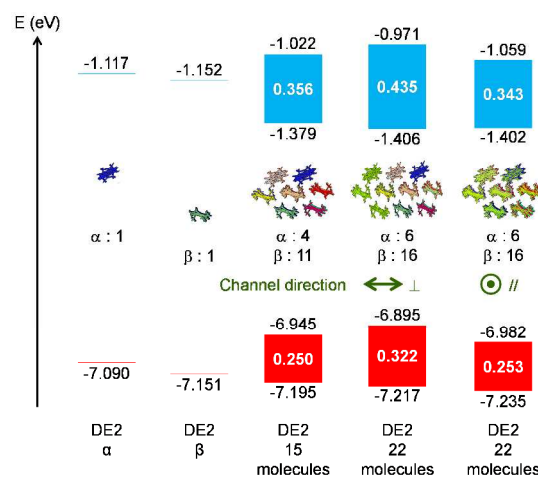


Fig. 9 HOMO and LUMO splittings calculated in 3-dimensional molecular clusters in a β layer in order to simulate the influence of the molecular orientation on the ambipolar charge transport properties of DE2 crystal.

splittings obtained in the first case indicates that ambipolar charge transport properties should be more effective in this configuration.

In order to clarify the role of the molecular orientation on the charge carrier mobilities, quantum chemical calculations were then performed for a 3D selection of DE2 molecules in both α and β layers. As shown in Fig. 9, the HOMO and LUMO splittings calculated for 15 DE2 molecules (4 α and 11 β molecules) were found to be 250 and 356 meV, respectively. This result confirms that DE2 is intrinsically an ambipolar organic semiconductor, which is in good agreement with the electrical properties of the DE2 OFETs with the parallel rubbing as well as with the quantum chemical calculations performed in dimers. We then looked at the influence of adding molecules in the appropriate directions on the splittings. When these additional molecules were placed sideways as indicated in Fig. 9, leading to a system with 6 α and 16 β DE2 molecules, both HOMO and LUMO splittings increased to 322 and 435 meV, respectively. In contrast, when additional molecules were placed in front and behind the initial 15 molecules shown in Fig. 9, the HOMO and LUMO splittings decreased to 253 and 343 meV. The first and second cases were calculated to simulate the effects of the

molecular orientation perpendicular and parallel to the OFET channel, respectively. The larger splitting values obtained for the perpendicular orientation suggest that the charge carrier mobilities should be higher in this direction, which seems to not be consistent with the experimental results obtained in DE2 OFETs. We can attribute this apparent discrepancy to the role played by charge trapping at grain boundaries on the charge transport properties of polycrystalline DE2 thin film devices. The density of grain boundaries is indeed larger when the grains are oriented perpendicular to the device channel. This implies that the decrease of the charge carrier mobilities due to charge trapping at the grain boundaries is presumably strongly reduced when the molecules and grains are aligned parallel to the channel.

Overall, this study shows that 3D quantum chemical calculations can be used to gain insights into the influence of the molecular orientation on the ambipolar charge transport properties of organic thin films. Our experimental results and our modeling provide evidence that the improved charge carrier mobilities in aligned DE2 OFETs are due to the intrinsic properties of the DE2 crystal. Nevertheless, it should be mentioned that the HOMO and LUMO splittings calculated in DE2 are on the same order of magnitude as those calculated in pentacene. As shown in the supplementary information section, the HOMO and LUMO splittings calculated for a 3D selection of 13 molecules in pentacene crystal exhibit values of 341 and 340 meV, respectively. This supports our conclusion that charge carrier mobilities in DE2 polycrystalline thin films are reduced by charge trapping at the grain boundaries.

Conclusion

In summary, we demonstrate that a preferential orientation of crystalline grains leads to a strong mobility enhancement and ambipolar transport in J-aggregate DE2 OFETs. Hole mobility anisotropy of about 20 is measured for drain current flowing parallel and perpendicular to the alignment direction. When the DE2 molecules are oriented parallel to the channel, we found that the devices become ambipolar with hole and electron mobilities, which can be as high as 0.01 and $7 \times 10^{-4} \text{ cm}^2 \text{ V}^{-1} \text{ s}^{-1}$, respectively. Quantum chemical calculations were carried out to elucidate the electronic structure of the DE2 crystal and determine the preferential directions for charge transport in the polycrystalline DE2 films. The results provide evidence that DE2 is intrinsically an ambipolar organic semiconductor and that charge trapping at the grain boundaries plays a key role on the charge transport properties of DE2 films. The enhancement of the hole mobilities by two orders of magnitude as well as the first observation of ambipolar transport in J-aggregate OFETs suggest that DE2 is an attractive material for organic electronic applications. Finally, improving the ambipolar charge transport properties in organic thin films by a control of the orientation of the crystalline grains is of interest for the realization of high mobility organic optoelectronic devices.

Acknowledgements

JCR acknowledges the support by the Basic Science Researcher Program and the Quantum Metamaterials Research Center (QMMRC) through the National Research Foundation of Korea (NRF) funded by the Ministry of Education, Science and Technology (grants 2011-0008650, 2012-0000543). TA acknowledges funding from the Japanese Society for the Promotion of Science via a JSPS KAKENHI grant (No. 22350084). The calculations were performed by using the RIKEN Integrated Cluster of Clusters (RICC) facility.

Notes and references

^a Department of Physics, CNRS-Ewha International Research Center, Ewha Womans University, Seoul 120-750, South Korea

^b Elements Chemistry Laboratory, RIKEN, 2-1 Hirosawa, Wako, Saitama 351-0198, Japan

^c Department of Environmental and Natural Sciences, Graduate School of Environment and Information Sciences, Yokohama National University, 79-2 Tokiwadai, Hodogaya-ku, Yokohama, Kanagawa 240-8501, Japan

^d Department of Chemistry and Biochemistry, Fukushima National College of Technology, 30 Aza-Nagao, Tairakamiarakawa, Iwaki, Fukushima 970-8034, Japan.

^e Department of Materials Science and Technology, Tokyo University of Science, 6-3-1 Nijjuku, Katsushika-ku, Tokyo 125-8585, Japan

^f Graduate School of Pharmaceutical Sciences, The University of Tokyo, 7-3-1 Hongo, Bunkyo-ku, Tokyo 113-0033, Japan

* To whom correspondence should be addressed.

E-mail: ribierre@opera.kyushu-u.ac.jp, taoyama@riken.jp, smatsu@ynu.ac.jp

† Electronic Supplementary Information (ESI) available: See DOI: 10.1039/b000000x/

- V. Coropceanu, J. Cornil, D.A. da Silva Filho, Y. Olivier, R. Silbey and J.L. Bredas, *Chem. Rev.* 2007, **107**, 926.
- J.L. Bredas, J.P. Calbert, D.A. da Silva Filho and J. Cornil, *Proc. Natl Acad. Sci. USA* 2002, **99**, 5804.
- J. Zaumseil and H. Sirringhaus, *Chem. Rev.* 2007, **107**, 1296.
- T. Okamoto, M.L. Senatore, M.M. Ling, A.B. Malik, M.L. Tang and Z. Bao, *Adv. Mater.* 2007, **19**, 3381.
- C. Kim, A. Facchetti and T.J. Marks, *Science* 2007, **318**, 76.
- H.A. Becerril, M.E. Roberts, Z. Liu, J. Locklin and Z. Bao, *Adv. Mater.* 2008, **20**, 2588.
- G. Giri, E. Verploegen, S.G.B. Mannsfeld, S. Atahan-Evrenk, D.H. Kim, S.Y. Lee, H.A. Becerril, A. Aspuru-Guzik, M.F. Toney and Z. Bao, *Nature* 2011, **480**, 504.
- J. Rivnay, L.H. Jimison, J.E. Northrup, M.F. Toney, R. Noriega, S. Lu, T.J. Marks, A. Facchetti and A. Salleo, *Nature Mater.* 2009, **8**, 952.
- L. Hartmann, K. Tremel, S. Uttiya, E. Crossland, S. Ludwigs, N. Kayunkid, C. Vergnat and M. Brinkmann, *Adv. Funct. Mater.* 2011, **21**, 4047.
- S. Nagamatsu, W. Takashima, K. Kaneto, Y. Yoshida, N. Tanigaki, K. Yase and K. Omote, *Macromolecules* 2003, **36**, 5252.
- Y. Hosokawa, M. Misaki, S. Yamamoto, M. Torii, K. Ishida and Y. Ueda, *Appl. Phys. Lett.* 2012, **100**, 203305.
- J.C. Ribierre, T. Fujihara, S. Watanabe, M. Matsumoto, T. Muto, A. Nakao and T. Aoyama, *Adv. Mater.* 2010, **22**, 1722.
- J.C. Ribierre, S. Watanabe, M. Matsumoto, T. Muto, A. Nakao and T. Aoyama, *Adv. Mater.* 2010, **22**, 4044.
- J.C. Ribierre, S. Watanabe, M. Matsumoto, T. Muto, and T. Aoyama, *Appl. Phys. Lett.* 2010, **96**, 083303.
- J.C. Ribierre, T. Fujihara, T. Muto, and T. Aoyama, *Appl. Phys. Lett.* 2010, **96**, 233302.
- J.C. Ribierre, S. Watanabe, M. Matsumoto, T. Muto, D. Hashizume, and T. Aoyama, *J. Phys. Chem. C* 2011, **115**, 20703.

- 17 S. Matsumoto, T. Kobayashi, T. Aoyama and T. Wada, *Chem. Comm.* 2003, 1910.
- 18 S. Matsumoto, K. Shirai, K. Kobayashi, T. Wada, and M.Z. Shiro, *Kristallogr.* 2004, **219**, 239.
- 19 T. Kobayashi, S. Matsumoto, T. Aoyama and T. Wada, *Thin Solid Films* 2006, **509**, 145.
- 20 T. Kobayashi, S. Matsumoto, T. Tanaka, H. Kunugita, K. Ema, T. Aoyama and T. Wada, *Phys. Chem. Chem. Phys.* 2005, **7**, 1726.
- 21 T. Tanaka, S. Matsumoto, T. Kobayashi, M. Sato and Aoyama, *J. Phys. Chem. C* 2011, **115**, 19598.
- 22 T. Tanaka, M. Sato, M. Ishitobi, T. Aoyama and S. Matsumoto, *Chem. Lett.* 2011, **40**, 1170.
- 23 K. Shirai, M. Matsuoka and K. Fukunishi, *Dyes Pigm.* 2000, **47**, 107.
- 24 T. Hosokai, T. Aoyama, T. Kobayashi, A. Nakao and S. Matsumoto, *Chem. Phys. Lett.* 2010, **487**, 77.
- 25 J.C. Ribierre, M. Sato, A. Ishizuka, T. Tanaka, S. Watanabe, M. Matsumoto, S. Matsumoto, M. Uchiyama and T. Aoyama, *Org. Electr.* 2012, **13**, 999.
- 26 J.C. Wittmann and P. Smith, *Nature* 1991, **352**, 414.
- 27 T. Tanaka, Y. Honda and M. Ishitobi, *Langmuir* 2001, **17**, 2192.
- 28 J. Baudrup and E.H. Immergut, Ed.: *Polymer Handbook*, 3rd Ed., Wiley, V/37, 1989.
- 29 S.E. Koh, C. Risko, D.A. da Silva Filho, O. Kwon, A. Facchetti, J.L. Bredas, T.J. Marks and M.A. Ratner, *Adv. Funct. Mater.* 2008, **18**, 332.
- 30 J. Cornil, J.P. Calbert, D. Beljonne, R. Silbey and J.L. Bredas, *Adv. Mater.* 2000, **12**, 978.
- 31 J. Cornil, J.P. Calbert and J.L. Bredas, *J. Am. Chem. Soc.* 2001, **123**, 1250.
- 32 D.A. da Silva Filho, E.G. Kim and J.L. Bredas, *Adv. Mater.* 2005, **17**, 1072.
- 33 M.J. Frisch, G.W. Trucks, H.B. Schlegel, G.E. Scuseria, M.A. Robb, J.R. Cheeseman, G. Scalmani, V. Barone, B. Mennucci, G.A. Petersson, H. Nakatsuji, M. Caricato, X. Li, H.P. Hratchian, A.F. Izmaylov, J. Bloino, G. Zheng, J.L. Sonnenberg, M. Hada, M. Ehara, K. Toyota, R. Fukuda, J. Hasegawa, M. Ishida, T. Nakajima, Y. Honda, O. Kitao, H. Nakai, T. Vreven, J.A. Montgomery, J.E. Peralta, F. Ogliaro, M. Bearpark, J.J. Heyd, E. Brothers, K.N. Kudin, V.N. Staroverov, T. Keith, R. Kobayashi, J. Normand, K. Raghavachari, A. Rendell, J.C. Burant, S.S. Iyengar, J. Tomasi, M. Cossi, N. Rega, J.M. Millam, M. Klene, J.E. Knox, J.B. Cross, V. Bakken, C. Adamo, J. Jaramillo, R. Gomperts, R.E. Stratmann, O. Yazyev, A.J. Austin, R. Cammi, C. Pomelli, J.W. Ochterski, R.L. Martin, K. Morokuma, V.G. Zakrzewski, G.A. Voth, P. Salvador, J.J. Dannenberg, S. Dapprich, A.D. Daniels, O. Farkas, J.B. Foresman, J.V. Ortiz, J. Cioslowski and D.J. Fox, *Gaussian 09*, revision C.01; Gaussian, Inc.: Wallingford, CT, 2010.
- 34 J. Zhang, Z. Ma, Q. Zhang, T. S. Virk, H. Geng, D. Wang, W. Xu, Z. Shuai, K. Singh, W. Hu and D. Zhu, *J. Mater. Chem. C* 2013, **1**, 5765.
- 35 G. Nan and Z. Li, *J. Mater. Chem. C* 2014, **2**, 1447.
- 36 G. te Velde, F.M. Bickelhaupt, E.J. Baerends, C. Fonseca Guerra, S.J.A. van Gisbergen, J.G. Snijders and T. Ziegler, *J. Comput. Chem.* 2001, **22**, 931.
- 37 S. Matsumoto, M. Satoh, D. Tsuchida, T. Kobayashi, T. Aoyama, T. Wada, *Trans. MRS-J* 2005, **30**, 345.
- 38 W.H. Lee, J.H. Cho and K. Cho, *J. Mater. Chem.* 2010, **20**, 2549.
- 39 S.Z. Weng, W.S. Hu, C.H. Kuo, Y.T. Tao, L.J. Fan and Y. W. Yang, *Appl. Phys. Lett.* 2006, **89**, 172103.
- 40 S.J. Kang, Y.Y. Noh, K.J. Baeg, J. Ghim, J.H. Park, D.Y. Kim, J.S. Kim, J.H. Park and K. Cho, *Appl. Phys. Lett.* 2008, **92**, 052107.
- 41 M.L. Swiggers, G. Xia, J.D. Slinker, A.A. Gorodetsky, G.G. Malliaras, R.L. Headrick, B.T. Weslowski, R.N. Shashidhar and C.S. Dulcey, *Appl. Phys. Lett.* 2001, **79**, 1300.
- 42 A. Di Carlo, F. Piacenza, A. Bolognesi, B. Stadlober and H. Maresh, *Appl. Phys. Lett.* 2005, **86**, 263501.
- 43 T. Matsushima, M. Yahiro and C. Adachi, *Appl. Phys. Lett.* 2007, **91**, 103505.
- 44 M.M. Ling, P. Erk, M. Koenemann, J. Locklin and Z. Bao, *Adv. Mater.* 2007, **19**, 1123.
- 45 Y. Wen, Y. Liu, C. Di, Y. Wang, X. Sun, Y. Guo, J. Zheng, W. Wu, S. Ye and G. Yu, *Adv. Mater.* 2009, **21**, 1631.
- 46 LUMO splitting of C₆₀ fullerene was calculated using the Hartree-Fock-based ZINDO/S method and using the CIF data of the fullerene, which can be obtained from the following database: <http://staff.aist.go.jp/nomura-k/japanese/itscgallery.htm>.